Farber Charles (Orcid ID: 0000-0002-6748-4711)
Clines Gregory (Orcid ID: 0000-0002-3755-7529)

# Osteoblasts Generate Testosterone from DHEA and Activate Androgen Signaling in Prostate Cancer Cells

Henry H. Moon[1], Katrina L. Clines[1], Patrick J. O'Day[1], Basel M. Al-Barghouthi[2], Emily A. Farber[2], Charles R. Farber[2,3], Richard J. Auchus[1,4], and Gregory A. Clines[1,4]

[1]Department of Internal Medicine, Division of Metabolism, Endocrinology & Diabetes, University of Michigan, Ann Arbor, Michigan

[2]Center for Public Health Genomics, University of Virginia, Charlottesville, Virginia

[3]Departments of Public Health Sciences, and Biochemistry and Molecular Genetics, University of Virginia, Charlottesville, Virginia

[4]Veterans Affairs Medical Center, Ann Arbor, Michigan

**Corresponding Author:**

Gregory A. Clines, M.D., Ph.D.

Associate Professor of Internal Medicine

Division of Metabolism, Endocrinology & Diabetes

Department of Internal Medicine

University of Michigan

Endocrinology Section, Ann Arbor VA Medical Center

2215 Fuller Road, Research 151

Ann Arbor, Michigan 48105-2399

Office: (734) 845-3443

Email: clines@umich.edu

**Abstract**

Bone metastasis is a complication of prostate cancer in up to 90% of men afflicted with advanced disease. Therapies that reduce androgen exposure remain at the forefront of treatment. However, most prostate cancers transition to a state whereby reducing testicular androgen action becomes ineffective. A common mechanism of this transition is intratumoral production of testosterone (T) using the adrenal androgen precursor dehydroepiandrosterone (DHEA) through enzymatic conversion by 3β- and 17β-hydroxysteroid dehydrogenases (3βHSD and 17βHSD). Given the ability of prostate cancer to form blastic metastases in bone, we hypothesized that osteoblasts might be a source of androgen synthesis. RNA expression analyses of murine osteoblasts and human bone confirmed that at least one 3βHSD and 17βHSD enzyme isoform was expressed, suggesting that osteoblasts are capable of generating androgens from adrenal DHEA. Murine osteoblasts were treated with 100 nM and 1 μM DHEA, or vehicle control. Conditioned media from these osteoblasts were assayed for intermediate and active androgens by liquid chromatography-tandem mass spectrometry. As DHEA was consumed, the androgen intermediates androstenediol and androstenedione were generated and subsequently converted to T. Conditioned media of DHEA-treated osteoblasts increased androgen receptor (AR) signaling, PSA production, and cell numbers of the androgen-sensitive prostate cancer cell lines C4-2B and LNCaP. DHEA did not induce AR signaling in osteoblasts despite AR expression in this cell type. We describe an unreported function of osteoblasts as a source of T that is especially relevant during androgen-responsive metastatic prostate cancer invasion into bone.

## Introduction

Bone metastases occur in up to 90% of men with advanced prostate cancer compared to significantly lower rates of skeletal metastases from other common cancers such as lung and colon [1]. The avidity of prostate cancer for bone suggests that the skeleton harbors factors in the bone microenvironment that foster prostate cancer growth [2]. Although work in this area has identified potential skeletal-derived factors that include bone morphogenetic proteins, wingless-integrated (Wnt)-signaling ligands, insulin-like growth factors, and transforming growth factor-β, none of these targets have shown promise to prevent and treat prostate cancer bone metastases [3-10].

The most well known factors necessary for prostate cancer growth are androgens. This observation was the basis for the development of androgen-deprivation therapies (ADT) to suppress testicular testosterone (T) production. ADT increases overall survival and progression-free survival in men with early castration-sensitive prostate cancer [11]. Unfortunately, most ADT-treated disease evolves into castration-resistant prostate cancer (CRPC), typically within two years after ADT initiation [12, 13]. A mechanism that CRPC cells commonly use to evade ADT is the intratumoral synthesis of androgens from the abundant circulating adrenal precursor dehydroepiandrosterone (DHEA) [14-17]. DHEA is produced in the adrenal cortex and is therefore unaffected by conventional ADT.

Dihydrotestosterone (DHT) is the most potent circulating androgen and is synthesized from T by peripheral tissues, with an affinity for the androgen receptor (AR) two to three times greater than T [18]. DHEA conversion to DHT requires three steroidogenic enzymes: 3β-hydroxysteroid dehydrogenase (3βHSD), 17β-hydroxysteroid dehydrogenase (17βHSD), and steroid 5α-reductase (SRD5α) (**Fig. 1**). Seven mouse and three human 3βHSD, at least fourteen 17βHSD (that includes proteins encoded by *AKR1C3* in humans, *Akr1c6* in mice, *RDH5*, and *RDH11*), and three SRD5α steroidogenic isoforms have been discovered, each with unique tissue expression patterns. Other groups have reported that osteoblasts express the three steroidogenic enzymes required for DHEA conversion to T and DHT [19-21]. Both T and DHT bind AR, which results in AR dimerization and translocation to the nucleus. The active androgen-AR complex then binds to androgen-response elements (AREs) and activates the transcription of androgen-responsive genes [22].

Mouse osteoblasts and human bone express at least one isoform of 17βHSD and 3βHSD. The skeleton may therefore generate androgens from DHEA, which represents an important mechanism for preferential growth of prostate cancer in bone and the formation of blastic rather than lytic metastases. We now report a novel mechanism by which the osteoblast utilizes DHEA as a substrate for active androgen synthesis that fuels prostate cancer androgen signaling and growth. This paracrine function of osteoblasts has not been reported previously and represents another example that the skeleton is a hormone-producing organ.



## Materials and Methods

### Harvest of murine osteoblasts

For primary calvarial osteoblast cultures, calvariae were harvested from 4-day-old ICR Swiss mouse pups, washed in phosphate-buffered saline (PBS), and then placed in PBS (2 mL per mouse litter) containing 0.1% collagenase (Wako Pure Chemical Industries, Osaka, Japan) and 0.2% dispase (Roche Applied Science, Penzberg, Germany). Calvariae were agitated at 37ºC for seven minutes to release cells. The first extraction was discarded, and the process was repeated three times. Osteoblasts collected in the last three extractions were combined. Cells were plated at a density of $10^6$ cells per 3.8 $cm^2$ in αMEM, 10% fetal bovine serum (FBS), 100 I.U./mL penicillin, and 100 µg/mL streptomycin.

Murine long bone osteoblasts were harvested using a modified protocol as previously described [23]. Femora, tibiae, and humeri were harvested from four- to six-week-old mice and thoroughly cleaned with a scalpel. Whole bones were subjected to a 20-minute digestion in digestion buffer at 37°C with shaking. This digestion was discarded, and the bones were subsequently washed three times in PBS. Any remaining tissue attached to the bones was removed to eliminate any potential contamination of other musculoskeletal cells. The epiphyseal/metaphyseal regions of the cleaned bones were removed, cut into smaller pieces, washed twice with PBS, and digested two hours at 37°C with shaking. Dispersed cells from this digest were collected by centrifugation and plated in αMEM with 10% FBS containing 100 I.U./mL penicillin and 100 µg/mL streptomycin. Osteoblasts are routinely cultured in hypoxia (5% $O_2$).

FBS that had been charcoal-stripped, a method to remove steroids, was used to culture osteoblasts during experimentation. Briefly, FBS was charcoal-stripped using a dextran-coated charcoal protocol [24]. Each batch completed this process three times, to ensure maximum removal of steroids.

Alizarin red staining of cultured osteoblasts

Cells were thawed and plated in a six-well plate in αMEM with 10% FBS containing 100 I.U./mL penicillin and 100 µg/mL streptomycin. The next day, half of the wells' media were treated with differentiation media containing osteoblast media with 10 mM beta-glycerol phosphate and 50 µg/mL ascorbic acid. Media from all wells were replaced every three days for 28 days. On the 28th day, the cells were washed carefully with PBS three times, fixed in 10% buffered formalin for 30 minutes, washed with distilled water twice, and stained with fresh 2% alizarin red (pH 4.2 with 10% ammonium hydroxide) for 5-10 minutes. The cells were carefully washed with copious amounts of water until no stain was observed in the wash.

RNA-Seq

Murine calvarial osteoblasts from four-day-old ICR Swiss pups were harvested. These cells were plated in triplicate in six-well plates and grown to confluence. The cells were washed with PBS, and frozen at -80° C. The RNA was isolated using a Zymo RNA MiniPrep Kit (Zymo Research, Irvine, CA). RNA integrity was evaluated using 0.1% bleach in a 1% agarose gel. RNA-Seq libraries were generated using the Illumina TruSeq Stranded mRNA prep kit (Illumina, San Diego, CA) and paired-end sequenced on a NextSeq 500/550 (Illumina, San Diego, CA) using an Illumina Nextseq High Output 150 cycle v2 cartridge. The reads were aligned to the GRCm38 genome assembly with hierarchical indexing for spliced alignment of transcripts (HISAT2) [25], then assembled and quantified with Stringtie [26]. Genes with less than six reads and 0.1 transcripts per million (TPM) in more than two samples were filtered.

Real-time RT-PCR

Long bone osteoblasts were cultured to confluence and RNA harvested using a Zymo RNA MiniPrep Kit (Zymo Research, Irvine, CA). Messenger RNA expression was determined by real-time RT PCR using an iScript SYBR Green RT-PCR kit (Bio-Rad, Hercules, CA) and a MyIQ Single-Color Real-Time PCR Detection

System (Bio-Rad, Hercules, CA). PCR primers are reported in the Supplemental Table. Relative differences in mRNA concentration were determined by subtracting the Ct (threshold cycle) of the study gene from the Ct of the housekeeping gene *Rpl32* ($\Delta = Ct_{gene} - Ct_{RPL32}$). The mean of the lowest enzyme isoform ($\Delta_{low}$) was subtracted from each cell type ($\Delta_{sample}$); (mean $\Delta_{low} - \Delta_{sample} = \varepsilon$). The fold difference was calculated as $2^{\varepsilon}$.

Cell lines and reagents

The prostate cancer cell lines C4-2B, LNCaP, and 22Rv1 were obtained from American Type Culture Collection (ATCC, Manassas, VA). The C4-2B and 22Rv1 cell lines were cultured in RPMI 1640 with 2 mM L-glutamine growth medium supplemented with 10% FBS. The LNCaP cell line was cultured in the same media as above but with the addition of 1 mM sodium pyruvate. The $ARCaP_M$ prostate cell line was obtained from Novicure Biotechnology (Birmingham, AL) and cultured in MCaP media (Novicure Biotechnology, Birmingham, AL) supplemented with 5% FBS. All cell lines were also cultured with 100 I.U./mL penicillin and 100 µl/mL streptomycin at 37°C containing 5% $CO_2$. DHEA was obtained from Steraloids (Newport, RI); R1881 was obtained from PerkinElmer (Waltham, MA); and enzalutamide was obtained from Selleck Chemicals (Houston, Texas). During experimentation, charcoal-stripped FBS was used.

Tandem mass spectrometry with two-dimensional liquid chromatography (LC-MS/MS)

Unlabeled and deuterium-labeled steroid standards were obtained from Sigma-Aldrich, Cerilliant, C/D/N Isotopes, and Cambridge Isotope Laboratories. A 20 µL aliquot of conditioned medium was diluted with 80 µL deionized water, mixed with internal standards, and extracted with 0.7 mL methyl-tert-butyl ether using Isolute cartridges (Biotage, Charlotte, NC) as described [27]. The 3-keto-delta-4-steroids and estrogens were quantitated directly using Agilent 1260 and 1290 dual front-end HPLC/UPLC equipped with 3 x 10 mm 5 µm particle size $C_4$ HypersilGOLD cartridge (Thermo Fisher), Kinetex 150mm x 2.1mm, 2.6 µm particle size biphenyl resolving column (Phenomenex, Torrance, CA), and an Agilent 6495 triple quadrupole mass spectrometer operating in electrospray ionization and multiple reaction monitoring (MRM) modes as described [27]. The 3-hydroxy-delta-5-steroids were quantitated after liquid-liquid extraction with methyl-tert-butyl ether and derivatization as picolinic acid esters, using a Kinetex 50 x 2.1 mm, 2.6 µm particle size biphenyl resolving column and an Agilent 6490 tandem mass spectrometer as described [28, 29].

Lentivirus transduction

The lentivirus pBM14-tat3-g.luc-VSVG (tat3-GLuc) construct was a gift from the Dr. William Rainey [30]. This reporter construct contains three AREs fused to a basal promoter and the *Gaussia* luciferase gene. The original tat3 AR reporter promoter was constructed previously [31]. *Gaussia* luciferase (GLuc) is a secreted luciferase allowing for collection and assay of media. The University of Michigan Vector Core provided the lentivirus 3.7DsRed-VSVG that constitutively expresses *Discosoma* red fluorescent protein (DsRed). Lentivirus stocks were diluted to 1X in a minimal volume of media with 6 µg/mL of polybrene added to the cultured cells. At ~50% confluent, cells were incubated with the 1X lentivirus overnight. The next morning, cultures were replaced with fresh medium and allowed to recover for 24 h before plating into experimental dishes.

AR-*Gaussia* reporter assay

Cells transduced with the tat3-Gluc/DsRed lentivirus combination were plated into 24-well black-walled, glass-bottom plates at 50% confluence. The cells were treated in quadruplicate. When conditioned media were collected, DsRed fluorescence was determined from each well using a BioTek Synergy HTX plate reader (BioTek, Winooski, VT), with the values used to normalize GLuc values. Conditioned media were collected and tested for GLuc activity using the GLuc substrate coelenterazine (Prolume, Pinetop, AZ). A 12 mM coelenterazine master stock was made with acidified methanol and stored at -80°C. The master stock was diluted in PBS containing 5 mM sodium chloride to make a 30 µM working stock. Fifty µL were injected into the wells of a solid white 96-well plate containing 20 µL of collected media from the transduced experimental cells. After a two second shaking, luminescence signal was integrated for 10 seconds and measured on a BioTek Synergy HTX plate reader (BioTek, Winooski, VT).

Prostate-specific antigen (PSA) enzyme-linked immunosorbent assay (ELISA)

Cells were plated into 24-well black walled, glass-bottom plates at 50% confluence. The cells were treated as with previous experiments in quadruplicate. PSA concentration of conditioned media was determined using human kallikrein 3/PSA Quantikine ELISA Kit (R&D Systems, Minneapolis, MN) on day 2 and 3, following the treatment. When conditioned media were collected, cell number was determined from each well using a

BioTek Lionheart FX automated microscope (BioTek, Winooski, VT) with the cell numbers, as measured by DsRed fluorescence, used to normalize PSA values.

Prostate cancer growth assays

Prostate cancer cells with constitutive DsRed expression were plated into 24-well black-walled, glass-bottom plates at 10% confluence. The cells were treated as with previous experiments in quadruplicate with treatments replenished at day 3. At day 0, 3 and 6, each well was imaged using a BioTek Lionheart FX automated microscope (BioTek, Winooski, VT) with a 4x/0.13NA objective (Olympus, Tokyo, Japan) and an RFP filter cube (531 nm/593 nm) paired with a 523 nm high power LED. The images were analyzed for confluency using the Gen5 Image Prime software package (BioTek, Winooski, VT).

Statistical analyses

Single variable data sets containing two groups were analyzed by a t-test. Single variable data sets containing three or more groups were analyzed by one-way ANOVA. Data sets containing two independent variables were analyzed by two-way ANOVA using Dunnett's, Sidak's or Tukey's multiple comparison testing. Data were analyzed using GraphPad Prism 9 Software (GraphPad Software, Inc., La Jolla, CA). An α-cutoff value of 0.05 was used for all analyses and reported p values were applied to two-tailed analyses.

**Results**

Osteoblasts express androgen steroidogenic enzymes

To test the hypothesis that osteoblasts metabolize DHEA into active androgens, we first assessed the expression of the required enzymes for these conversions. The expression of each of these enzymes was determined using three complementary methods—RNA-Seq of cultured murine calvarial osteoblasts (**Fig. 2A**), RT-PCR of murine long bone osteoblasts from male and female mice (**Suppl. Fig. 2**), and analysis of public RNA-Seq data from a human cohort of iliac crest bone biopsies from 58 healthy female subjects (**Fig. 2B**) [32]. At least one isoform of the three enzymes was expressed in the mouse and human samples. The patterns of

*HSD17B* isoform expression were remarkably similar between the two murine and one human expression datasets, with *HSD17B4*, *HSD17B10*, *HSD17B11*, *HSD17B12*, and *RDH11* having consistent expression across the three datasets. *SRD5A1* and *SRD5A3* were also expressed among the murine osteoblasts and human bone samples. A single gene isoform of *HSD3B—HSD3B7*—was abundantly expressed in mouse osteoblasts and human bone. Differences in expression between male and female long bone osteoblasts were detected, although the overall pattern of isoenzyme expression remained the same. The striking similarities between mouse and human expression existed despite the likely presence of bone cells other than osteoblasts present in the human bone marrow samples.

The expression of *Cyp19a1*, the gene that encodes aromatase that generates estradiol from T and estrone from androstenedione, was not detected in murine calvarial osteoblasts via RNA-Seq or long bone osteoblasts via real-time RT-PCR expression analyses (data not shown). Human *CYP19A1* message was reported present in the iliac crest bone biopsy samples but in a very low amount with a mean gene count of 29.8 (SD ± 14.0). Gene counts of less than 10 were reported as being non-expressed [32]. This level of expression was similar to other steroidogenesis genes with the lowest gene counts such as *HSD17B3* and *HSD17B6*.

Osteoblasts generate active androgens from DHEA

Murine osteoblasts harvested from the epiphyseal region of long bones were selected for study (**Suppl. Fig. 1**). To assess osteoblast metabolism of DHEA, confluent murine osteoblast cultures were treated with 100 nM and 1 μM DHEA and compared to an ethanol vehicle control. Conditioned media (CM) were collected 24, 48, and 72 h later and analyzed by LC-MS/MS. As the DHEA concentration declined, androstenediol and androstenedione increased with peak concentrations of 36,716 and 253 pg/mL (~127 and 1 nM), respectively, at 48 h with the 1 μM DHEA treatment (**Fig. 3**). DHEA was preferentially converted to androstenediol, rather than androstenedione since the peak concentration of androstenediol was more than ten times greater than androstenedione in both the 100 nM and 1 μM DHEA treatment groups. The peak concentration of T was 101 pg/mL (0.3 nM) at 72 h with the 1 μM DHEA treatment. The synthesis of androstenedione from DHEA and T from androstenediol by the only 3βHSD enzyme expressed, 3βHSD7, may be a rate-limiting step in the conversion of DHEA to active androgens. Despite *Srd5a* expression, DHT was not detected with the 1 μM DHEA treatment at any timepoint (data now shown).

Neither estradiol nor estrone was detected in DHEA-treated osteoblast conditioned media by LC-MS/MS. The lower limit of detection of these estrogens in this sensitive assay is 4.9 pg/mL and is consistent with negligible *Cyp19a1* expression in murine osteoblasts.

Prostate cancer generation of androgens from DHEA

The prostate cancer cell lines LNCaP and C4-2B are androgen sensitive [33]. The ability of these cell lines to generate androgens from DHEA was compared to two androgen-insensitive prostate cancer cell lines, 22Rv1 and $ARCaP_M$. LNCaP, C4-2B, 22Rv1, and $ARCaP_M$ cells were transduced with a lentivirus expressing a constitutively active red fluorescent protein (DsRed) as a normalization control for any potential cellular proliferative effects of the treatments. After transduction, cells were treated with 100 nM DHEA. Media were collected 72 h later and assayed for DHEA, androstenediol, androstenedione, T, and DHT by LC-MS/MS (**Fig. 4**).

LNCaP and C4-2B cells demonstrated active 3βHSD activity with robust conversion of DHEA to androstenedione. Less activity was detected in 22Rv1 and $ARCaP_M$ cells. Significant androstenediol was detected in 22Rv1 and $ARCaP_M$, and less in C4-2B and LNCaP. C4-2B generated significant T followed by 22Rv1, LNCaP, and $ARCaP_M$. DHT was only detected in C4-2B media. In contrast to 22Rv1 and $ARCaP_M$, LNCaP and C4-2B cells efficiently metabolized DHEA.

Conditioned media of osteoblasts treated with DHEA activate prostate cancer AR signaling

The capacity for osteoblast-generated T to activate AR signaling in prostate cancer cells was next tested. Since the androgen-sensitive prostate cancer cells also synthesize androgens from DHEA, the contributions of each cell type to generate androgens were determined. Residual T already present in osteoblast conditioned media (CM) would immediately activate prostate cancer AR signaling, whereas DHEA must first be converted to T or DHT in prostate cancer cells before AR signaling would commence.

The prostate cancer cell lines LNCaP and C4-2B were transduced with a lentivirus AR-reporter construct (tat3-GLuc) containing three AREs fused to a basal promoter and *Gaussia* luciferase (GLuc) [31]. GLuc is a secreted protein that allows for easy collection of media over time as a measure of androgen receptor signaling activation. The cells were also transduced with a lentivirus constitutively expressing DsRed, with fluorescence

used to normalize GLuc values to relative cell number. The androgen analog R1881 robustly increased GLuc activity in both LNCaP and C4-2B prostate cancer cell lines (**Suppl. Fig. 3**). The ability of osteoblast CM to activate prostate cancer AR signaling was next examined (**Fig. 5**). CM was collected from murine long bone osteoblasts 72 h after treatment with 100 nM and 1 μM DHEA, or an ethanol vehicle control. More immediate increases in GLuc were expected from T already present in DHEA-treated osteoblast CM compared to direct DHEA treatment of the prostate cancer cells. After prostate cancer cells were transduced with the tat3-Gluc/DsRed lentivirus combination, the media were replaced with 50% of the respective prostate cancer medium and 50% CM from osteoblasts that had been treated with 100 nM DHEA, 1 μM DHEA, or ethanol vehicle control. These groups were compared to the prostate cancer cells treated directy with 100 nM DHEA, 1 μM DHEA, or ethanol vehicle control along with 50% osteoblast CM treated with EtOH. As expected, the groups treated with ethanol vehicle CM or ethanol vehicle directly did not show AR signaling activation (**Fig. 6**). In both LNCaP and C4-2B cell lines, treatment with 100 nM DHEA CM versus 100 nM DHEA, and 1 μM DHEA CM versus 1 μM DHEA resulted in significantly more AR signaling activation at 12, 24, 36, and 48 h. Continued differences were detected in the LNCaP cell line at 72 h. In the C4-2B cell line, 100 nM DHEA treatment at 72 h resulted in even greater AR signaling activation compared to the 100 nM DHEA CM group. At 1 μM DHEA CM compared to 1 μM DHEA treatment, the degree of AR signaling activation was similar.

Enzalutamide blocks prostate cancer AR signaling induced by osteoblast-generated androgen

Enzalutamide is an effective and specific androgen antagonist that blocks three AR activation steps: androgen binding to AR, translocation of the androgen-AR complex to the nucleus, and the assocation of the androgen-AR complex to AREs [34]. To demonstrate the specificity of DHEA-treated osteoblast CM acting through AR signaling, the ability of enzalutamide to block AR signaling was tested. C4-2B prostate cancer cells were transduced with the tat3-GLuc/DsRed lentivirus combination and treated with and without 1 μM enzalutamide daily, as well as 100 nM DHEA CM (**Fig. 7A**), 1 μM DHEA CM (**Fig. 7B**), or ethanol vehicle control. Enzalutamide significantly blocked AR signaling of cells treated with 100 nM DHEA CM and 1 μM DHEA CM at 48 and 72 hours. These data indicate specific AR signaling activation of prostate cancer cells by osteoblast-generated androgens.

Conditioned media of osteoblasts treated with DHEA increase prostate PSA production and cell number

The ability of osteoblast-generated androgens to stimulate PSA production by LNCaP and C4-2B cells was tested. The prostate cancer cells were transduced with the DsRed lentivirus, to monitor cell number, and treated with 100 nM DHEA CM or 100 nM DHEA, 1 μM DHEA CM or 1 μM DHEA, and compared to EtOH CM and an ethanol vehicle control. Media were collected at 48 and 72 hours. LNCaP (**Fig. 8A, B**) and C4-2B (**Fig. 8C, D**) showed a marked increase in PSA production in both DHEA CM concentrations. Although PSA did not increase with DHEA direct treatment in the LNCaP cells, it did increase in the C4-2B cells compared to vehicle controls.

Prostate cancer cell growth also responded to osteoblast-generated androgens. Prostate cancer cells were transduced with the DsRed lentivirus and treated with 100 nM DHEA CM or 100 nM DHEA, 1 μM DHEA CM or 1 μM DHEA, and compared to EtOH CM and an ethanol vehicle control. DsRed fluorescence, as a marker of cell number, was measured by fluorescence microscopy and reported as percent culture confluence after three and six days of culture. Treatment with 100 nM DHEA CM and 1 μM DHEA CM compared to EtOH CM increased cell number in LNCaP (**Fig. 9A, B**) and C4-2B (**Fig. 9C, D**) cells. The increase was blocked with daily 1 μM enzalutamide treatment, except in C4-2B cells with the 1 μM DHEA CM treatment. The response to DHEA CM compared to direct DHEA treatment differed among cells. In LNCaP cells, the growth response of the 1 μM DHEA CM treatment was greater than the 1 μM DHEA treament; no difference was detected with the 100 nM treatment groups. In C4-2B cells, 100 nM DHEA CM increased cell number compared to 100 nM DHEA treatment. However, the reverse was true with the higher 1 μM DHEA direct treatment compared to 1 μM DHEA CM.

DHEA does not activate osteoblast AR signaling

The concentration of T generated by conversion of the lowest DHEA concentration in osteoblasts would be expected to activate androgen signaling, as the equilibrium dissociation constant of the AR for T is ~0.2 nM (58 pg/mL) [18]. It has been reported that AR is expressed in osteoblasts, osteocytes, osteoclasts, and many other cell types present in the bone microenvironment [35]. We confirmed that AR is expressed in murine osteoblast cultures (data not shown). When tat3-GLuc/DsRed transduced osteoblasts were treated with R1881, a modest

increase in GLuc was detected (**Fig. 10**). However, DHEA at 100 nM and 1 μM did not increase GLuc expression.

**Conclusion**

A novel and unreported discovery that the osteoblast generates androgens from the adrenal steroid precursor DHEA is now reported. This finding represents another example that the skeleton is a true hormone-producing organ. It remains unclear the extent to which the skeleton contributes to circulating androgens, but the concentration of testosterone generated is sufficient to activate AR signaling locally. Osteoblasts may therefore represent an essential source of androgens to fuel prostate cancer bone metastases, complementing or fulfilling androgen production when intratumoral androgen generation by prostate cancer cells may be limited or absent. The affinity of prostate cancer cells to the skeleton is a phenomenon that is unique compared to many other types of cancer. The bone microenvironment creating a rich source of androgens is a plausible explanation for prostate cancers' affinity towards invasion and growth in the skeleton.

The intratumoral generation of androgens is an important mechanism of CRPC progression [14-17]. However, the frequency and degree in which this phenomenon occurs, especially in bone metastasis, are unknown. Variability in intratumoral androgen production is due to inherited genetic variation and changes in steroidogenesis enzyme expression during carcinogenesis [36-40]. The four prostate cancer cells reported here represent examples of such variability, as each has unique androgen generating characteristics. Although C4-2B was the only cell line that generated DHT, it is likely that intratumoral generation of T without DHT is sufficient to direct CRPC growth [38, 41]. The clinical relevance is that in early bone metastasis, when single or clusters of prostate cancer cells first invade bone, the shear larger number of osteoblasts would contribute to more local androgen production than the prostate cancer cells. As bone metastasis progresses, the contribution of prostate cancer-generated androgens would then depend not only on cell numbers, but also on the capacity of these prostate cancer cells to generate androgens.

To investigate how osteoblast-generated androgens contribute to prostate cancer AR signaling and growth, a strategy was selected in which CM from osteoblasts after DHEA treatment was compared to the direct

treatment of DHEA. Since osteoblasts did not completely metabolize all DHEA, and androstenediol and androstenedione intermediates were also present in the CM, these substrates likely contributed to the intratumoral generation of androgens by prostate cancer cells. However, since enzymatic conversion of these substrates by the prostate cancer cells takes time, the greater increase in AR signaling with the CM at the earlier timepoints is due to osteoblast-generated testosterone.

While osteoblast-generated androgens, as reported here, likely contribute to prostate cancer expansion in bone, other mechanisms of prostate cancer regulation by osteoblasts have been reported. In one report, co-culture with the pre-osteoblast cell line MC3T3 accentuated the DHT-regulated increase in MDA-PCa-2b prostate cancer cell numbers [42]. CM from MC3T3 cells also increased the expression of *AR* and the steroidogenesis enzymes *HSD3B1*, *AKR1C3*, *SRD5A1* in the CRPC cell line LNCaP-19 leading to an increase in intratumoral androgen production and a possible increase in AR sensitivity [43]. Furthermore, the CM of human primary osteoblast cultures was reported to increase PSA production of LNCaP cells in the absence of steroid treatment. Although a similar result was not found in the data presented here, this may suggest differences between human and mouse primary osteoblast cultures [44].

The LNCaP and C4-2B prostate cancer cells were selected for further study due to the responsiveness to osteoblast-generated androgens. They were also selected for their dissimilarities in androgen production. Although LNCaP cells had a comparable ability to generate testosterone as osteoblasts, the generation of testosterone did not keep pace with testosterone present in the osteoblast CM. The LNCaP prostate cancer cell line demonstrated greater AR signaling, PSA secretion and cell numbers with DHEA CM treatments compared to DHEA added directly to the culture media. C4-2B cells, however, displayed different kinetics to osteoblast CM. At earlier timepoints and with the 100 nM CM treatment, there was a trend for greater AR signaling, PSA production, and cell growth. However, C4-2B AR signaling activation at later timepoints and at the higher 1 μM DHEA direct treatment outpaced the androgen present in osteoblast CM. This was likely due to the robust conversion of DHEA to testosterone and especially DHT in this cell line. Both cell lines demonstrated a rapid increase in PSA production with the DHEA CM treatments since PSA is a robust, early indicator of AR activation, as previously reported [45, 46]. In contrast, the increase in cell numbers with the DHEA CM treatments is a confirmatory but slower sign of androgen action [47, 48].

The effects of DHEA and R1881 on AR signaling were also investigated in osteoblasts. Despite osteoblasts generating T from DHEA, AR signaling was not increased compared to vehicle control. Although the concentration of T was sufficient for AR binding, the absence of DHT in the CM of DHEA-treated osteoblasts was a possible contributor. Osteoblasts lack the expression of *Srd5a2* that encodes an enzyme with an affinity for T that is 14-20 times greater than the enzyme encoded by *Srdr5a1* [49, 50]. The kinetics of the enzyme encoded by *Srd5a3* are unknown. R1881 did increase AR signaling modestly above the vehicle control. These data indicate that the murine osteoblasts harvested from the ends of long bones, specifically the epiphyseal and metaphyseal regions, are not highly sensitive to androgens, despite AR expression. Although osteoblasts have been reported to be targets of androgens [42], this is not true with osteoblasts in all skeletal compartments. The skeletal phenotype of osteoblast-targeted genetic deletion of *Ar* has been reported by a number of groups [51-54]. The consensus among these reports is that trabecular bone but not cortical bone osteoblasts are sensitive to AR actions in both sexes. Since at least a partial response to R1881 was detected, it is likely that the osteoblasts harvested and reported here are a mixture of cortical and trabecular osteoblasts.

An unexpected finding is that only a single 3βHSD enzyme isoform was expressed in mouse osteoblasts and human bone. The 3βHSD7 enzyme may, therefore, serve as a unique drug target to block osteoblast androgen production and prostate cancer bone metastasis in CRPC. Targeting this isoenzyme, which has more tissue-selective expression, would be expected to have fewer adverse effects than targeting other proteins, such as AR, which has more global expression. Mice engineered for *Hsd3b7* inactivation die of hepatic failure due to the participation of 3βHSD7 in hepatic bile acid synthesis. However, most of these mice, when maintained on vitamin and bile acid supplements, had a normal lifespan [55]. Mutations in human *HSD3B7* cause congenital defects in bile acid synthesis [56, 57]. While *HSD3B1*, another 3βHSD isoenzyme gene, participates in the resistance to androgen-deprivation therapy in prostate cancer patients [36], a role for HSD3B7 in prostate cancer or the skeleton has not been reported.

During the initial invasion of prostate cancer cells to bone, the osteoblast may be the principal source of androgens. This hypothesis has not been directly tested since clinical trials have not been designed to address this question. The pivotal clinical trials evaluating the androgen synthesis inhibitor abiraterone acetate and the androgen receptor antagonist enzalutamide reported an increase in overall survival and clinical progression-free survival when combined with ADT and compared to ADT alone in patients with metastatic prostate cancer,

most of who had bone metastasis [58-60]. However, these studies combined the radiographic progression of bone metastasis with other criteria for progression, such as symptomatic skeletal events and progression of soft-tissue tumors. Data reporting solely radiographic progression of bone metastases are unavailable. The results of these clinical trials do not illuminate the extent to which osteoblast-generated androgens promote bone metastasis. Although a separate clinical study reported that abiraterone acetate reduced androgen concentrations in bone marrow collected from men with prostate cancer bone metastases, the individual contributions of the prostate cancer cells and osteoblasts to androgen production remain unclear [61].

Although estrogens contribute to prostate cancer progression [62], neither expression of the *Cyp19a1* gene that encodes for aromatase nor estradiol in CM was detected in murine osteoblasts. A small amount of *CYP19A1* was reported in human iliac bone biopsy samples [32]. These human samples were not a pure osteoblast population, and other cell types were likely present that included bone marrow adipocytes that express *CYP19A1* [63].

This report also has implications for skeletal development during adrenarche. Adrenarche commences between the ages of five and eight in girls and boys and is the period when the adrenal zona reticularis initiates secretion of DHEA and 11-oxygenated $C_{19}$ steroids [64, 65]. Select tissues convert adrenal DHEA to androgens, including the pubic hair follicles, sweat glands, and the liver. While significant effects of androgens on the skeleton occur during puberty, bone maturation begins during adrenarche before the onset of puberty despite the lack of adequate gonadal T production [66-68], possibly due to the intracrine generation of sex steroids from adrenal-derived precursors. Although circulating adrenal 11-ketotestosterone and other androgens are responsible for the androgenic manifestations of normal and premature adrenarche [69], the osteoblast may be central to local generation of skeletal androgens and subsequent conversion to sex steroids from DHEA before the start of puberty. Local generation of androgens and estrogens may also serve as a protective mechanism to mitigate bone loss during male and female hypogonadism. At the cellular level, T increases osteoblast proliferation and osteocyte function [53, 54, 70].

We now propose a novel model in which the osteoblast receives adrenal precursor steroids and metabolizes these into androgenic prostate cancer growth factors. This model implies that targeting osteoblast steroidogenic enzymes might be an effective treatment for prostate cancer bone metastases.

**Acknowledgements**

This work was funded by a Department of Veterans Affairs Merit Award (I01 BX001370) to GC, and a University of Michigan Integrative Musculoskeletal Health Core Center Pilot & Feasibility award (NIH P30 AR069620) to GC. BA was supported in part by a National Institutes of Health, Biomedical Data Sciences Training Grant (5T32LM012416). Authors' roles: Study design: HM, RA, and GC. Study conduct: HM, KC, PO'D, EF. Data collection: HM, KC, PO'D, EF. Data analysis: HM, KC, BA, CR, RA, and GC. Data interpretation: HM, KC, CF, RA, and GC. Drafting manuscript: HM, KC, and GC. Revising manuscript content: All authors. Approving final version of manuscript: All authors. GC takes responsibility for the integrity of the data analysis. The authors have no conflicts of interest.

**References**


1. Bubendorf L, Schopfer A, Wagner U, et al. Metastatic patterns of prostate cancer: an autopsy study of 1,589 patients. Hum Pathol. 2000;31(5):578-83.
2. Sowder ME, Johnson RW. Bone as a Preferential Site for Metastasis. JBMR Plus. 2019;3(3):e10126.
3. Weilbaecher KN, Guise TA, McCauley LK. Cancer to bone: a fatal attraction. Nat Rev Cancer. 2011;11(6):411-25.
4. Ihle CL, Straign DM, Provera MD, Novitskiy SV, Owens P. Loss of Myeloid BMPR1a Alters Differentiation and Reduces Mouse Prostate Cancer Growth. Front Oncol. 2020;10:357.
5. Hall CL, Bafico A, Dai J, Aaronson SA, Keller ET. Prostate cancer cells promote osteoblastic bone metastases through Wnts. Cancer Research. 2005;65(17):7554-60.
6. Clines GA, Mohammad KS, Bao Y, et al. Dickkopf homolog 1 mediates endothelin-1-stimulated new bone formation. Molecular Endocrinology. 2007;22:486-98.
7. Dai J, Hall CL, Escara-Wilke J, Mizokami A, Keller JM, Keller ET. Prostate cancer induces bone metastasis through Wnt-induced bone morphogenetic protein-dependent and independent mechanisms. Cancer Res. 2008;68(14):5785-94.
8. Kimura T, Kuwata T, Ashimine S, et al. Targeting of bone-derived insulin-like growth factor-II by a human neutralizing antibody suppresses the growth of prostate cancer cells in a human bone environment. Clin Cancer Res. 2010;16(1):121-9.
9. Wan X, Li ZG, Yingling JM, et al. Effect of transforming growth factor beta (TGF-β) receptor I kinase inhibitor on prostate cancer bone growth. Bone. 2012;50(3):695-703.
10. Fournier PG, Juarez P, Jiang G, et al. The TGF-β Signaling Regulator PMEPA1 Suppresses Prostate Cancer Metastases to Bone. Cancer Cell. 2015;27(6):809-21.

11. Seidenfeld J, Samson DJ, Hasselblad V, et al. Single-therapy androgen suppression in men with advanced prostate cancer: a systematic review and meta-analysis. Annals of Internal Medicine. 2000;132(7):566-77.
12. Eisenberger MA, Blumenstein BA, Crawford ED, et al. Bilateral orchiectomy with or without flutamide for metastatic prostate cancer. N Engl J Med. 1998;339(15):1036-42.
13. Karantanos T, Corn PG, Thompson TC. Prostate cancer progression after androgen deprivation therapy: mechanisms of castrate resistance and novel therapeutic approaches. Oncogene. 2013;32(49):5501-11.
14. Dillard PR, Lin MF, Khan SA. Androgen-independent prostate cancer cells acquire the complete steroidogenic potential of synthesizing testosterone from cholesterol. Mol Cell Endocrinol. 2008;295(1-2):115-20.
15. Auchus RJ. The backdoor pathway to dihydrotestosterone. Trends Endocrinol Metab. 2004;15(9):432-8.
16. Chang KH, Ercole CE, Sharifi N. Androgen metabolism in prostate cancer: from molecular mechanisms to clinical consequences. Br J Cancer. 2014;111(7):1249-54.
17. Auchus RJ, Sharifi N. Sex Hormones and Prostate Cancer. Annu Rev Med. 2020;71:33-45.
18. Grino PB, Griffin JE, Wilson JD. Testosterone at high concentrations interacts with the human androgen receptor similarly to dihydrotestosterone. Endocrinology. 1990;126(2):1165-72.
19. Kuwano Y, Fujikawa H, Watanabe A, et al. 3Beta-hydroxysteroid dehydrogenase activity in human osteoblast-like cells. Endocr J. 1997;44(6):847-53.
20. Feix M, Wolf L, Schweikert HU. Distribution of 17beta-hydroxysteroid dehydrogenases in human osteoblast-like cells. Mol Cell Endocrinol. 2001;171(1-2):163-4.
21. Saito H, Yanaihara T. Steroid formation in osteoblast-like cells. J Int Med Res. 1998;26(1):1-12.
22. Davey RA, Grossmann M. Androgen Receptor Structure, Function and Biology: From Bench to Bedside. Clin Biochem Rev. 2016;37(1):3-15.

23. Bakker AD, Klein-Nulend J. Osteoblast isolation from murine calvaria and long bones. Methods Mol Biol. 2012;816:19-29.
24. SigmaAldrich. Preparation of charcoal-stripped fetal bovine serum 2020 [Available from: https://www.sigmaaldrich.com/content/dam/sigma-aldrich/docs/Sigma/Usage/f2442use.pdf.
25. Kim D, Langmead B, Salzberg SL. HISAT: a fast spliced aligner with low memory requirements. Nat Methods. 2015;12(4):357-60.
26. Pertea M, Pertea GM, Antonescu CM, Chang TC, Mendell JT, Salzberg SL. StringTie enables improved reconstruction of a transcriptome from RNA-seq reads. Nat Biotechnol. 2015;33(3):290-5.
27. Wright C, O'Day P, Alyamani M, Sharifi N, Auchus RJ. Abiraterone acetate treatment lowers 11-oxygenated androgens. Eur J Endocrinol. 2020;182(4):413-21.
28. Davio A, Woolcock H, Nanba AT, et al. Sex Differences in 11-Oxygenated Androgen Patterns Across Adulthood. J Clin Endocrinol Metab. 2020;105(8):e2921-9.
29. Banker M, Puttabyatappa M, O'Day P, et al. Association of Maternal-Neonatal Steroids with Early Pregnancy Endocrine Disrupting Chemicals and Pregnancy Outcomes. J Clin Endocrinol Metab. 2020;106(3):665-87.
30. Campana C, Rege J, Turcu AF, et al. Development of a novel cell based androgen screening model. J Steroid Biochem Mol Biol. 2016;156:17-22.
31. Chen S, Wang J, Yu G, Liu W, Pearce D. Androgen and glucocorticoid receptor heterodimer formation. A possible mechanism for mutual inhibition of transcriptional activity. J Biol Chem. 1997;272(22):14087-92.
32. Farr JN, Roforth MM, Fujita K, et al. Effects of Age and Estrogen on Skeletal Gene Expression in Humans as Assessed by RNA Sequencing. PLoS One. 2015;10(9):e0138347.
33. Wu TT, Sikes RA, Cui Q, et al. Establishing human prostate cancer cell xenografts in bone: induction of osteoblastic reaction by prostate-specific antigen-producing tumors in athymic and

SCID/bg mice using LNCaP and lineage-derived metastatic sublines. Int J Cancer. 1998;77(6):887-94.

34. Tran C, Ouk S, Clegg NJ, et al. Development of a second-generation antiandrogen for treatment of advanced prostate cancer. Science. 2009;324(5928):787-90.
35. Almeida M, Laurent MR, Dubois V, et al. Estrogens and Androgens in Skeletal Physiology and Pathophysiology. Physiol Rev. 2017;97(1):135-87.
36. Hearn JWD, AbuAli G, Reichard CA, et al. HSD3B1 and resistance to androgen-deprivation therapy in prostate cancer: a retrospective, multicohort study. Lancet Oncol. 2016;17(10):1435-44.
37. Stanbrough M, Bubley GJ, Ross K, et al. Increased expression of genes converting adrenal androgens to testosterone in androgen-independent prostate cancer. Cancer Res. 2006;66(5):2815-25.
38. Montgomery RB, Mostaghel EA, Vessella R, et al. Maintenance of intratumoral androgens in metastatic prostate cancer: a mechanism for castration-resistant tumor growth. Cancer Res. 2008;68(11):4447-54.
39. Uemura M, Tamura K, Chung S, et al. Novel 5 alpha-steroid reductase (SRD5A3, type-3) is overexpressed in hormone-refractory prostate cancer. Cancer science. 2008;99(1):81-6.
40. Hofland J, van Weerden WM, Dits NF, et al. Evidence of limited contributions for intratumoral steroidogenesis in prostate cancer. Cancer Res. 2010;70(3):1256-64.
41. Titus MA, Schell MJ, Lih FB, Tomer KB, Mohler JL. Testosterone and dihydrotestosterone tissue levels in recurrent prostate cancer. Clin Cancer Res. 2005;11(13):4653-7.
42. Liu XH, Kirschenbaum A, Yao S, Liu G, Aaronson SA, Levine AC. Androgen-induced Wnt signaling in preosteoblasts promotes the growth of MDA-PCa-2b human prostate cancer cells. Cancer Res. 2007;67(12):5747-53.
43. Hagberg Thulin M, Nilsson ME, Thulin P, et al. Osteoblasts promote castration-resistant prostate cancer by altering intratumoral steroidogenesis. Mol Cell Endocrinol. 2016;422:182-91.

44. Blaszczyk N, Masri BA, Mawji NR, et al. Osteoblast-derived factors induce androgen-independent proliferation and expression of prostate-specific antigen in human prostate cancer cells. Clinical Cancer Research. 2004;10(5):1860-9.
45. Kampa M, Papakonstanti EA, Hatzoglou A, Stathopoulos EN, Stournaras C, Castanas E. The human prostate cancer cell line LNCaP bears functional membrane testosterone receptors that increase PSA secretion and modify actin cytoskeleton. FASEB J. 2002;16(11):1429-31.
46. Zhu YS, Cai LQ, You X, Cordero JJ, Huang Y, Imperato-McGinley J. Androgen-induced prostate-specific antigen gene expression is mediated via dihydrotestosterone in LNCaP cells. J Androl. 2003;24(5):681-7.
47. Song W, Khera M. Physiological normal levels of androgen inhibit proliferation of prostate cancer cells in vitro. Asian J Androl. 2014;16(6):864-8.
48. Yu P, Duan X, Cheng Y, et al. Androgen-independent LNCaP cells are a subline of LNCaP cells with a more aggressive phenotype and androgen suppresses their growth by inducing cell cycle arrest at the G1 phase. Int J Mol Med. 2017;40(5):1426-34.
49. Normington K, Russell DW. Tissue distribution and kinetic characteristics of rat steroid 5 alpha-reductase isozymes. Evidence for distinct physiological functions. J Biol Chem. 1992;267(27):19548-54.
50. Peng HM, Valentin-Goyco J, Im SC, et al. Expression in Escherichia Coli, Purification, and Functional Reconstitution of Human Steroid 5$\alpha$-Reductases. Endocrinology. 2020;161(8):1-11.
51. Notini AJ, McManus JF, Moore A, et al. Osteoblast deletion of exon 3 of the androgen receptor gene results in trabecular bone loss in adult male mice. J Bone Miner Res. 2007;22(3):347-56.
52. Chiang C, Chiu M, Moore AJ, et al. Mineralization and bone resorption are regulated by the androgen receptor in male mice. J Bone Miner Res. 2009;24(4):621-31.
53. Maatta JA, Buki KG, Ivaska KK, et al. Inactivation of the androgen receptor in bone-forming cells leads to trabecular bone loss in adult female mice. Bonekey Rep. 2013;2:440.

54. Sinnesael M, Claessens F, Laurent M, et al. Androgen receptor (AR) in osteocytes is important for the maintenance of male skeletal integrity: evidence from targeted AR disruption in mouse osteocytes. J Bone Miner Res. 2012;27(12):2535-43.
55. Shea HC, Head DD, Setchell KD, Russell DW. Analysis of HSD3B7 knockout mice reveals that a 3$\alpha$-hydroxyl stereochemistry is required for bile acid function. Proc Natl Acad Sci U S A. 2007;104(28):11526-33.
56. Schwarz M, Wright AC, Davis DL, Nazer H, Bjorkhem I, Russell DW. The bile acid synthetic gene 3$\beta$-hydroxy-$\Delta^5$-$C_{27}$-steroid oxidoreductase is mutated in progressive intrahepatic cholestasis. J Clin Invest. 2000;106(9):1175-84.
57. Cheng JB, Jacquemin E, Gerhardt M, et al. Molecular genetics of 3$\beta$-hydroxy-$\Delta^5$-$C_{27}$-steroid oxidoreductase deficiency in 16 patients with loss of bile acid synthesis and liver disease. J Clin Endocrinol Metab. 2003;88(4):1833-41.
58. Fizazi K, Carducci M, Smith M, et al. Denosumab versus zoledronic acid for treatment of bone metastases in men with castration-resistant prostate cancer: a randomised, double-blind study. Lancet. 2011;377(9768):813-22.
59. Davis ID, Martin AJ, Stockler MR, et al. Enzalutamide with Standard First-Line Therapy in Metastatic Prostate Cancer. N Engl J Med. 2019;381(2):121-31.
60. Armstrong AJ, Szmulewitz RZ, Petrylak DP, et al. ARCHES: A Randomized, Phase III Study of Androgen Deprivation Therapy With Enzalutamide or Placebo in Men With Metastatic Hormone-Sensitive Prostate Cancer. J Clin Oncol. 2019;37(32):2974-86.
61. Efstathiou E, Titus M, Tsavachidou D, et al. Effects of abiraterone acetate on androgen signaling in castrate-resistant prostate cancer in bone. J Clin Oncol. 2012;30(6):637-43.
62. Dobbs RW, Malhotra NR, Greenwald DT, Wang AY, Prins GS, Abern MR. Estrogens and prostate cancer. Prostate Cancer Prostatic Dis. 2019;22(2):185-94.

63. Amanatullah DF, Tamaresis JS, Chu P, et al. Local estrogen axis in the human bone microenvironment regulates estrogen receptor-positive breast cancer cells. Breast Cancer Res. 2017;19(1):121.
64. Turcu AF, Nanba AT, Chomic R, et al. Adrenal-derived 11-oxygenated 19-carbon steroids are the dominant androgens in classic 21-hydroxylase deficiency. Eur J Endocrinol. 2016;174(5):601-9.
65. O'Reilly MW, Kempegowda P, Jenkinson C, et al. 11-Oxygenated C19 Steroids Are the Predominant Androgens in Polycystic Ovary Syndrome. J Clin Endocrinol Metab. 2017;102(3):840-8.
66. Sopher AB, Thornton JC, Silfen ME, et al. Prepubertal girls with premature adrenarche have greater bone mineral content and density than controls. J Clin Endocrinol Metab. 2001;86(11):5269-72.
67. Sopher AB, Jean AM, Zwany SK, et al. Bone age advancement in prepubertal children with obesity and premature adrenarche: possible potentiating factors. Obesity (Silver Spring). 2011;19(6):1259-64.
68. Utriainen P, Laakso S, Liimatta J, Jaaskelainen J, Voutilainen R. Premature adrenarche--a common condition with variable presentation. Horm Res Paediatr. 2015;83(4):221-31.
69. Rege J, Turcu AF, Kasa-Vubu JZ, et al. 11-Ketotestosterone Is the Dominant Circulating Bioactive Androgen During Normal and Premature Adrenarche. J Clin Endocrinol Metab. 2018;103(12):4589-98.
70. Ucer S, Iyer S, Bartell SM, et al. The Effects of Androgens on Murine Cortical Bone Do Not Require AR or ERalpha Signaling in Osteoblasts and Osteoclasts. J Bone Miner Res. 2015;30(7):1138-49.

**Figure Legends**

**Figure 1. Generation of androgens from adrenal DHEA**. The conversion of DHEA to dihydrotestosterone (DHT) involves the enzymes 3β-hydroxysteroid dehydrogenase (3βHSD), 17β-hydroxysteroid dehydrogenase (17βHSD), and steroid 5α-reductase (SRD5α).

**Figure 2. Expression of androgenic steroidogenesis enzymes in bone**. The mRNA expression of *HSD3B*, *HSD17B*, and *SRD5A* isoforms was determined. The x-axis indicates the genetic isoform of each enzyme. (**A**) Murine calvarial osteoblasts were harvested from a mixed population of male and female 4-day-old mouse pups and subjected to RNA-Seq analyses. (**B**) RNA-Seq expression is reported from iliac crest bone biopsies from 58 healthy women [32]. Expression values from individual subjects are indicated. The y-axes indicate the number of counts identified from each gene. All data points, mean, interquartile range, and the minimum/maximum values are indicated as box plots. Statistical differences in mRNA concentration compared to the gene with the lowest mRNA counts within each isoform (indicated as "REF") are reported using one-way ANOVA with Dunnett's multiple comparison test. Statistical p values greater than 0.10 are not shown. A6 = *Akr1c6*, A3 = *AKR1C3*, R5 = *RDH5*, R11 = *RDH11*.

**Figure 3. Osteoblasts generate androgenic steroids from DHEA**. Murine osteoblasts were harvested from a pooled mixture of male and female long bone epiphyses. Osteoblast cultures were treated with 100 nM or 1 μM DHEA and compared to an ethanol vehicle control group. Conditioned media collected at 24, 48, and 72 h after initiation of treatments were analyzed for DHEA, androstenedione, androstenediol, and testosterone concentrations by LC-MS/MS. Medium alone containing 100 nM or 1 μM DHEA, or ethanol was also analyzed for contamination with downstream metabolites, and the results are indicated at the 0 h timepoint. All data points are reported. The connecting lines indicate the mean at each timepoint. Individual steroid concentrations significantly changed over time with both the 100 nM and 1 μM DHEA treatment groups as determined by one-way ANOVA (DHEA: $p<0.001$, $p<0.001$; androstenedione: $p=0.007$, $p<0.001$; androstenediol: $p=0.002$, $p<0.001$; testosterone: $p=0.002$, $p<0.001$). The pairwise differences between the 1 μM and 100 nM DHEA and EtOH treatment groups were determined and reported using two-way ANOVA. EtOH = ethanol.

**Figure 4. DHEA increases the production of androgenic steroids by human prostate cancer cell lines**. The human prostate cancer cell lines LNCaP, C4-2B, 22Rv1, and $ARCaP_M$ were cultured and treated with 100 nM DHEA. Media were collected 72 h after treatment and analyzed for DHEA, androstenedione, androstenediol, testosterone, and dihydrotestosterone (DHT) concentration by LC-MS/MS. All data points are reported. The connecting lines indicate the mean at each timepoint. The data were analyzed using two-way ANOVA with Tukey's multiple comparison test. The significant differences reported are a comparison to the cell line with the lowest steroid concentration. Statistical p values greater than 0.10 are not shown.

**Figure 5. Scheme to generate osteoblast conditioned media.** Murine long bone osteoblasts were treated with 100 nM or 1 μM DHEA, or an EtOH vehicle control. Osteoblast conditioned media (CM) were collected 72 h later. Prostate cancer cells were then treated with EtOH vehicle-treated fresh media only (**EtOH**), 50% EtOH CM and 50% EtOH vehicle-treated fresh media (**EtOH CM**), 50% EtOH CM and 50% DHEA-treated fresh media (**100 nM/1 μM DHEA**), or 50% DHEA CM and 50% EtOH vehicle-treated fresh media (**100 nM/1 μM DHEA CM**). After specified times, prostate cancer media were collected for analyses. Treatment scheme created with BioRender.com.

**Figure 6. Conditioned media of DHEA-treated osteoblasts increase AR signaling in prostate cancer cells**. Murine long bone osteoblasts were treated with 100 nM and 1 μM DHEA or an ethanol vehicle control for 72 h, and conditioned media (CM) were collected. LNCaP and C4-2B cell lines were transduced with the tat3-Gluc/DsRed lentivirus combination and then treated with the osteoblast CM, 100 nM DHEA (**A**, **C**), or 1 μM DHEA (**B**, **D**). These groups were compared to ethanol vehicle control osteoblast CM and to ethanol vehicle added directly to the media as illustrated in Figure 5. Prostate cancer conditioned media were collected at 12, 24, 36, 48, and 72 h, analyzed for GLuc activity, and normalized to cell number using DsRed fluorescence. All data points are reported. The connecting lines indicate the mean at each timepoint. LNCaP and C4-2B GLuc production increased significantly over time in the 100 nM and 1 μM DHEA CM, and 100 nM and 1 μM DHEA treatment groups as determined by one-way ANOVA ($p<0.001$ for all groups). Pairwise

differences between treatment groups were determined using two-way ANOVA (**E**). RLU = relative light units, RFU = relative fluorescent units, CM = osteoblast conditioned media, EtOH = ethanol.

**Figure 7. Enzalutamide blocks AR signaling of C4-2B prostate cancer cells treated with conditioned media of DHEA-treated osteoblasts.** The C4-2B prostate cancer cell line was cultured and transduced with the tat3-Gluc/DsRed lentivirus combination. The cells were then treated with and without 1 μM of the AR antagonist enzalutamide daily, and with conditioned media (CM) from osteoblasts treated with 100 nM DHEA (**A**), 1 μM DHEA (**B**), and an ethanol vehicle control for 72 h. Media were collected at 48 and 72 h, analyzed for GLuc activity, and normalized to cell number using DsRed fluorescence. All data points are reported. The connecting lines indicate the mean at each timepoint. The data were analyzed using two-way ANOVA. Statistical differences are only reported for comparisons between the DHEA CM and DHEA CM + enzalutamide treatment groups. RLU = relative light units, RFU = relative fluorescence units, CM = osteoblast conditioned media, EtOH = ethanol, ENZ = enzalutamide.

**Figure 8. Conditioned media of DHEA-treated osteoblasts increase PSA secretion of prostate cancer cells**. The human prostate cancer cell lines LNCaP (**A, B**) and C4-2B (**C, D**) were treated with an EtOH vehicle control (EtOH), or conditioned media from murine long bone osteoblasts treated with an EtOH vehicle control (EtOH CM), 100 nM (100 nM DHEA CM), or 1 μM DHEA (1 μM DHEA CM). Media were collected at 48 and 72 hours and compared to a medium-only control. PSA concentration in the conditioned media was determined by ELISA and normalized to prostate cancer cell number. Cell number was determined by DsRed expression. All data points are reported. The connecting lines indicate the mean at each timepoint. Pairwise differences were determined using two-way ANOVA. Statistical p values greater than 0.10 are not shown. CM = osteoblast conditioned media, EtOH = ethanol.

**Figure 9. Conditioned media of DHEA-treated osteoblasts increase prostate cancer cell number.** The human prostate cancer cell lines LNCaP (**A, B**) and C4-2B (**C, D**) were transduced with a DsRed lentivirus and treated with an EtOH vehicle control (EtOH), conditioned media from murine long bone osteoblasts treated with an EtOH vehicle control (EtOH CM), 100 nM (100 nM DHEA CM), or 1 μM DHEA (1 μM DHEA CM). The 100

nM DHEA CM and 1 μM DHEA CM groups were also treated daily with and without 1 μM enzalutamide. DsRed fluorescence was measured at days 0, 3 and 6 by fluorescence microscopy and reported as percent culture confluence. All data points are reported. The connecting lines indicate the mean at each timepoint. Pairwise differences were determined using two-way ANOVA (**E**). CM = osteoblast conditioned media, EtOH = ethanol, ENZ = enzalutamide.

**Figure 10. DHEA does not increase AR signaling in osteoblasts**. Murine long bone osteoblasts were transduced with the tat3-Gluc/DsRed lentivirus combination. Cells were treated with 100 nM and 1 μM DHEA and compared to 10 nM of the synthetic androgen R1881 or an ethanol vehicle control. Conditioned media were analyzed for GLuc activity and normalized to cell number using DsRed fluorescence (**A**). All data points are reported. The connecting lines indicate the mean at each timepoint. Pairwise differences were determined using two-way ANOVA (**B**). RLU = relative light units, RFU = relative fluorescence units.

**Supplemental Figure 1. Staining of long bone osteoblasts with alizarin red.** The identity of long bone osteoblasts harvested from the epiphyses was confirmed with the accumulation of mineralized matrix with long-term, 28**-**day, culture in osteoblast differentiation media.

**Supplemental Figure 2. Expression of androgenic steroidogenesis enzymes in murine long bone osteoblasts.** The x-axis indicates the genetic isoform of each enzyme. Osteoblasts were collected from male and female murine long bones epiphyses. RNA was prepared and underwent real-time RT-PCR analyses. The y-axis indicates relative expression values. All data points, mean, and the minimum/maximum values are indicated. Statistical differences in mRNA concentration between male (M) and female (F) mRNA concentration of each gene are reported using two-way ANOVA with Sidak's multiple comparison test. Statistical p values greater than 0.10 are not shown. A6 = *Akr1c6*, R5 = *Rdh5*, R11 = *Rdh11*.

**Supplemental Figure 3. R1881 increases AR signaling in prostate cancer cells.** The human androgen-sensitive prostate cancer cell lines LNCaP and C4-2B were cultured and transduced with the tat3-Gluc/DsRed

lentivirus combination. LNCaP (**A**) and C4-2B (**B**) cell lines were treated with 10 nM R1881. Media were collected at 12, 24, 48, and 72 h, and analyzed for GLuc activity to confirm androgen responsiveness. The differences between treatment groups were determined using two-way ANOVA. EtOH = ethanol.

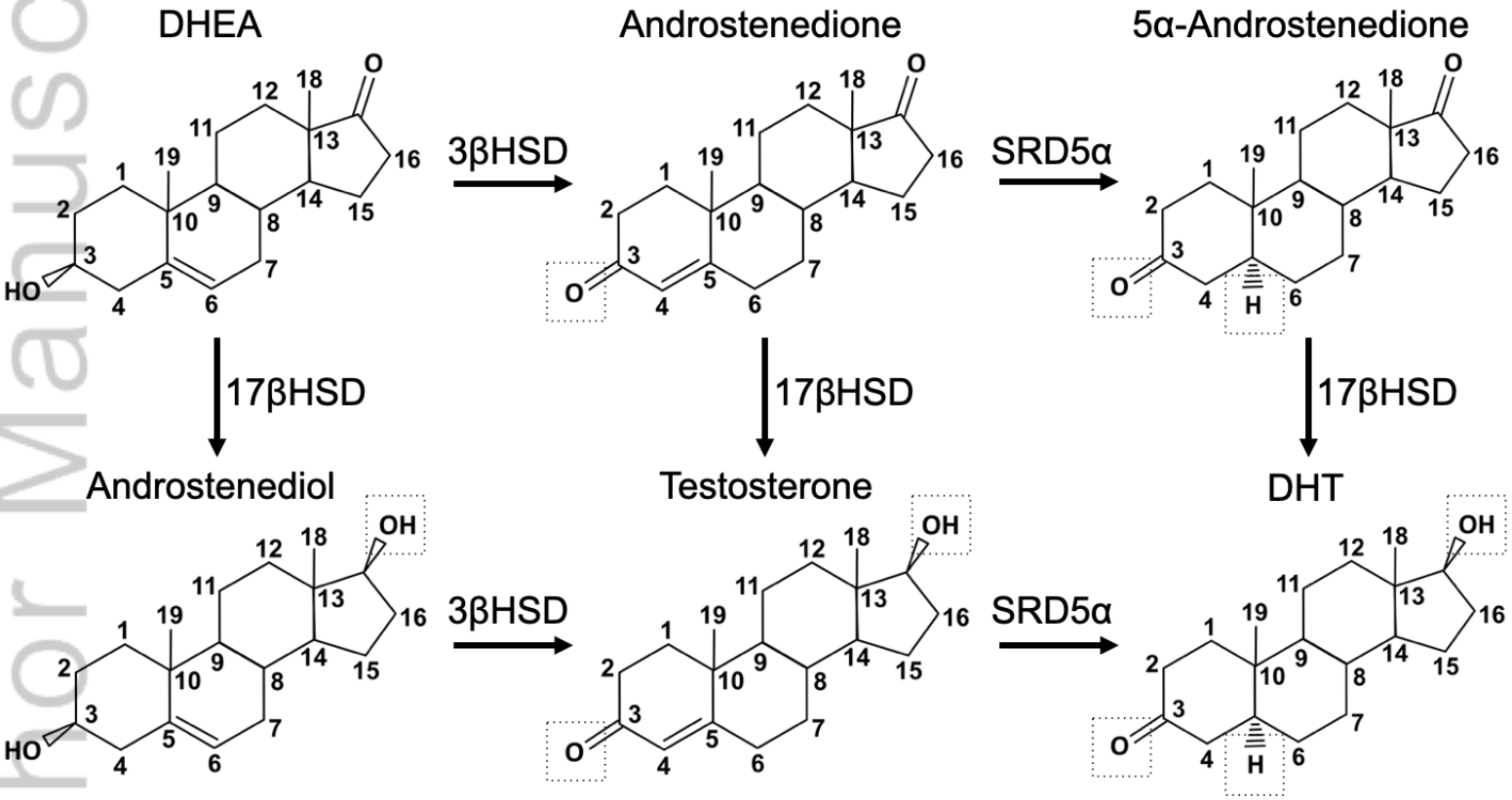


JBMR_4313_Figure 1.tiff

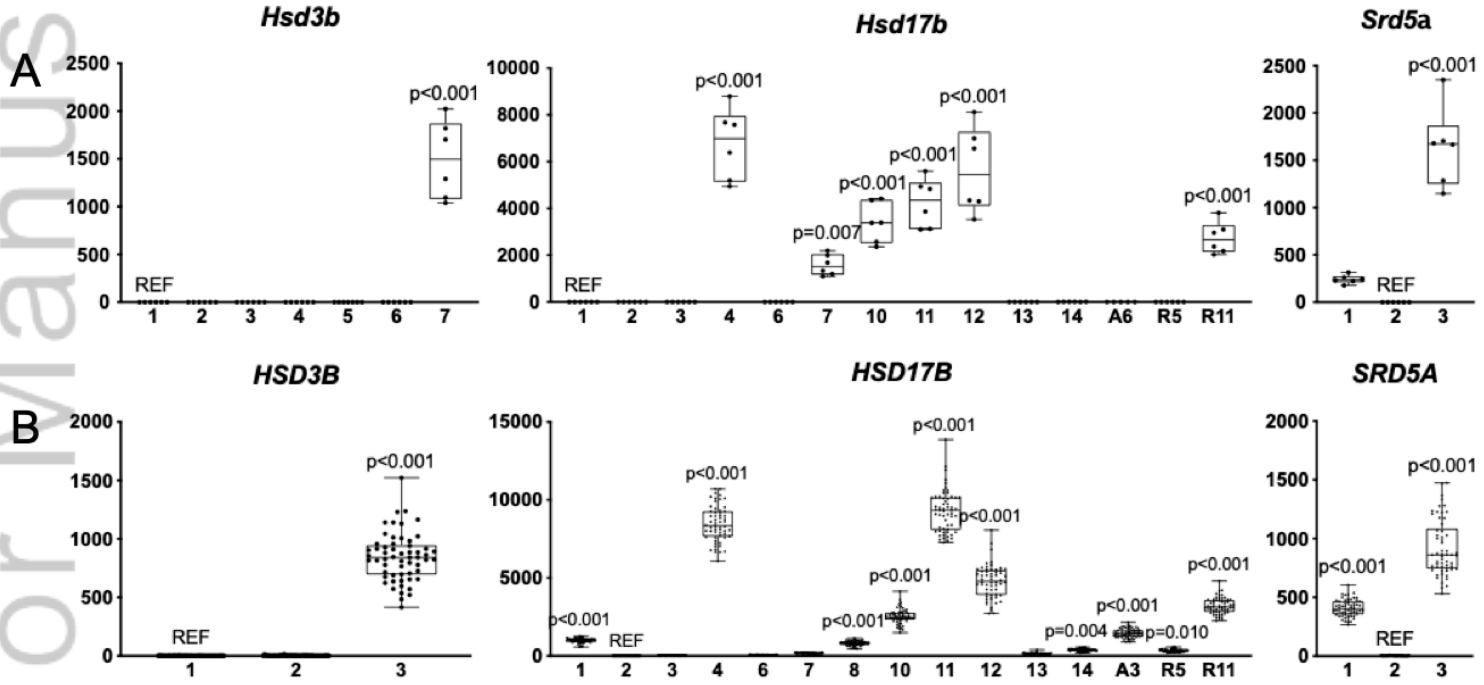


JBMR_4313_Figure 2.tiff

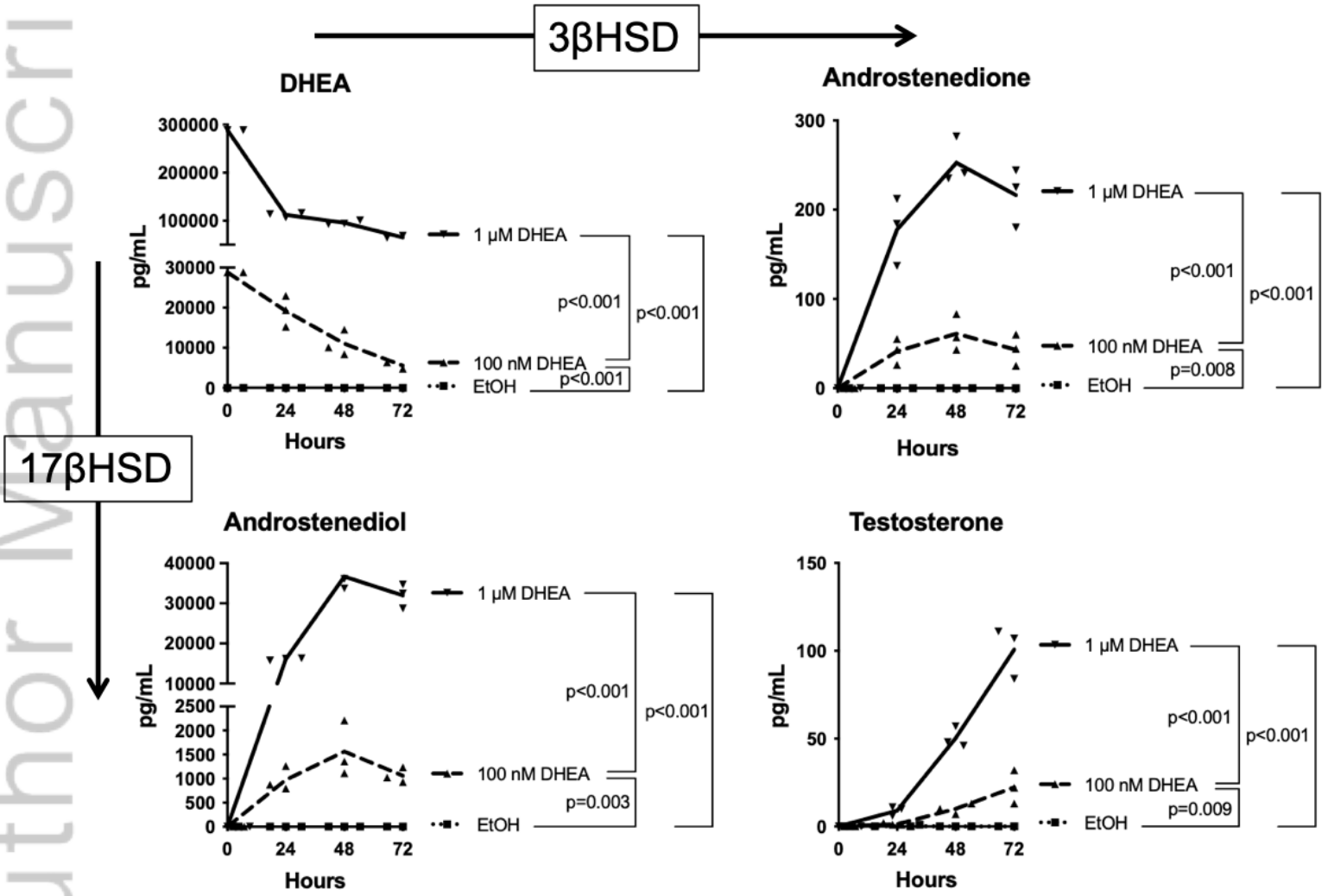


JBMR_4313_Figure 3.tiff

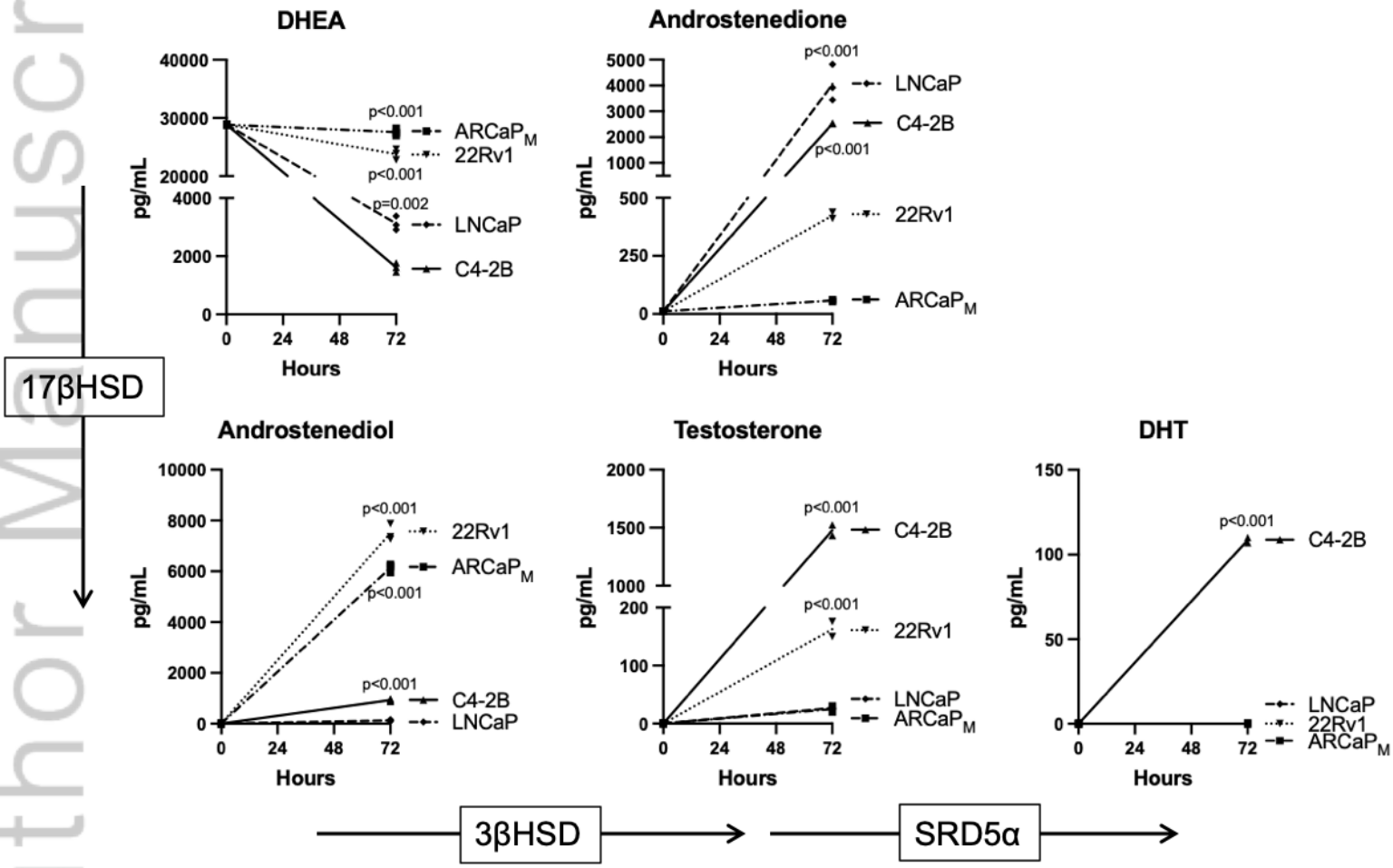


JBMR_4313_Figure 4.tiff

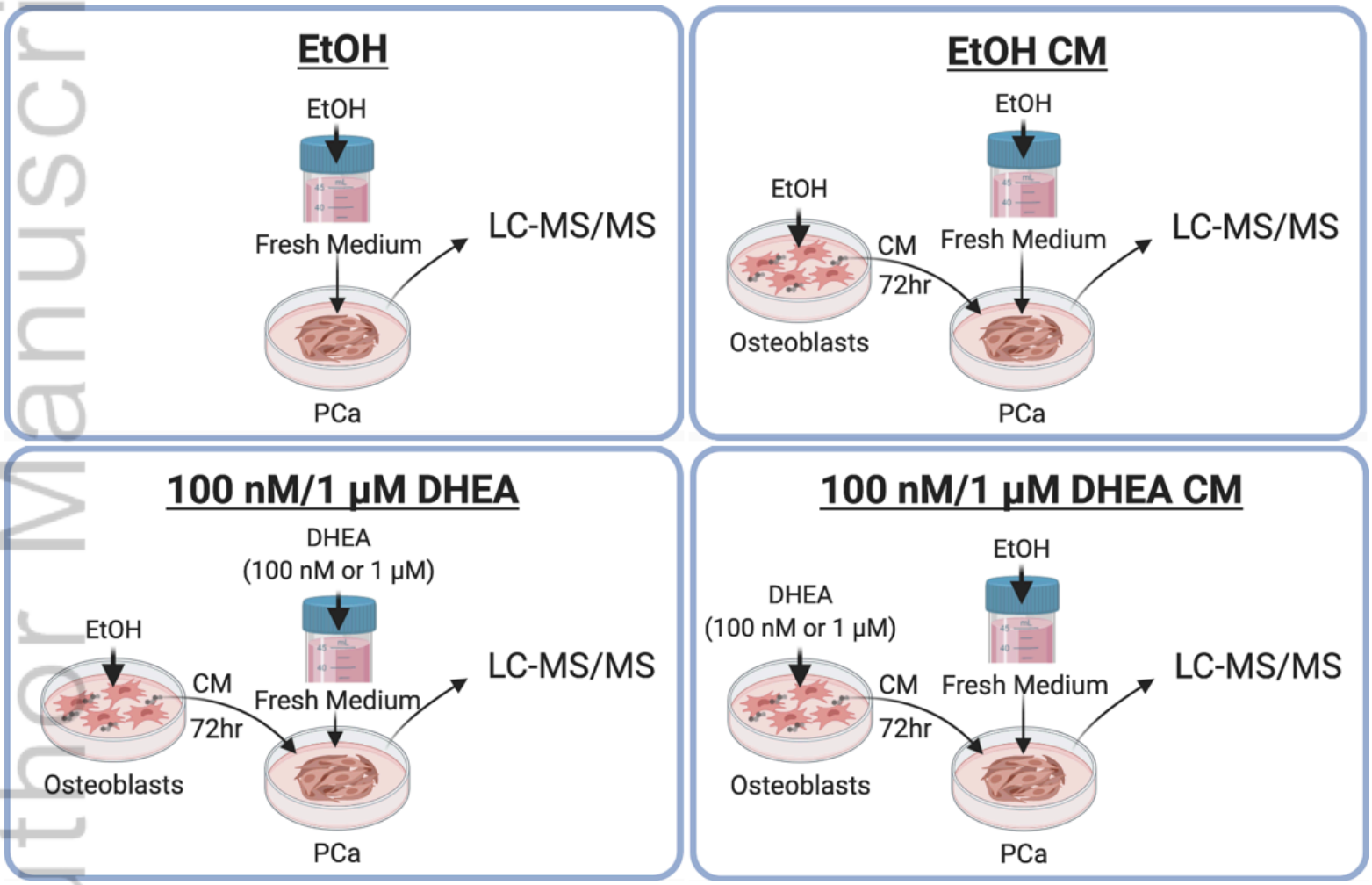


JBMR_4313_Figure 5.tiff

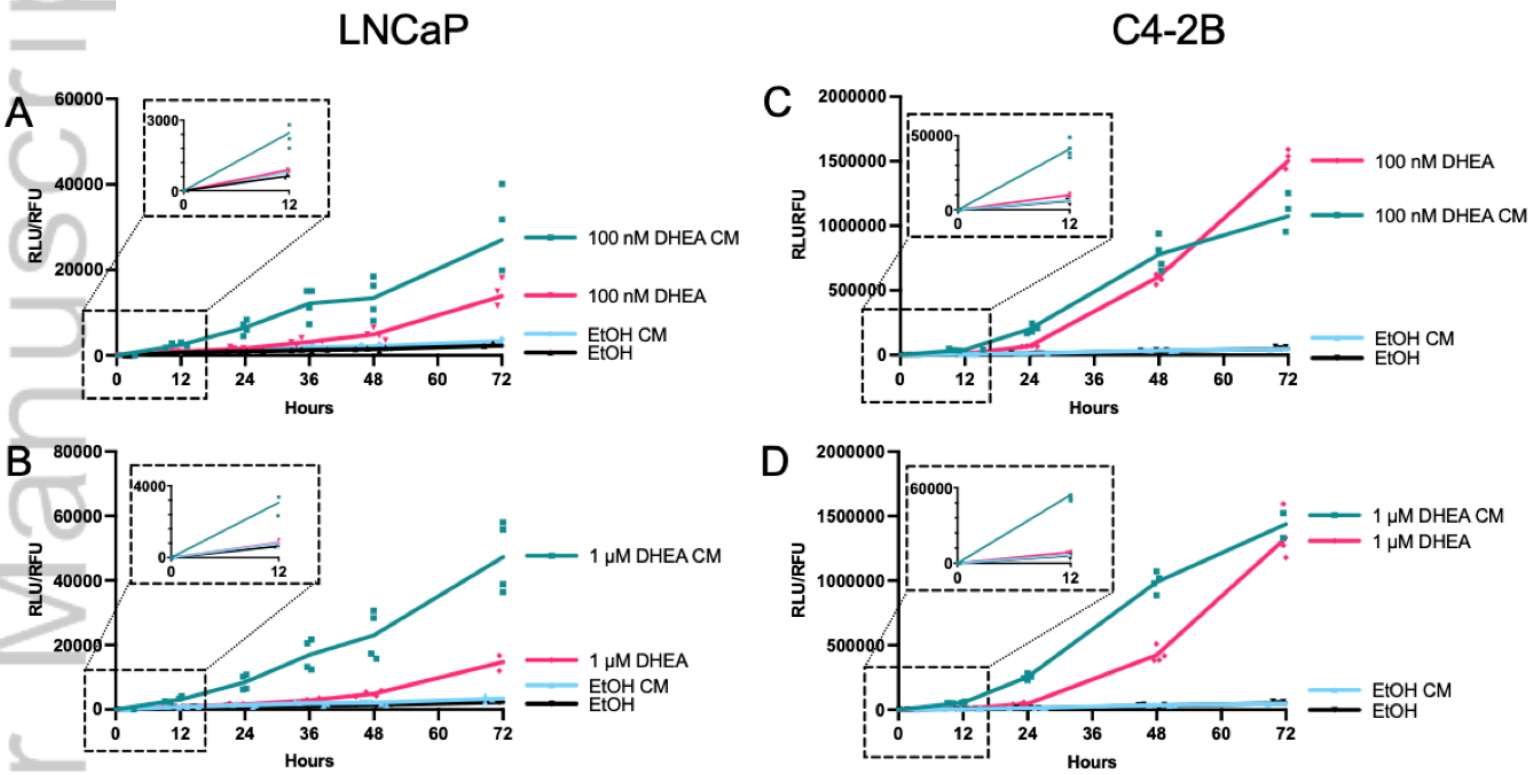


E

| Pairwise treatment comparisons vs. | | p value LNCaP | p value C4-2B |
|---|---|---|---|
| EtOH CM | 100 nM DHEA CM | **0.003** | **<0.001** |
| EtOH CM | 1 μM DHEA CM | **<0.001** | **<0.001** |
| 100 nM DHEA CM | 1 μM DHEA CM | 0.073 | **0.013** |
| 100 nM DHEA | 100 nM DHEA CM | **0.016** | >0.1 |
| 1 μM DHEA | 1 μM DHEA CM | **0.002** | **0.001** |

JBMR_4313_Figure 6.tiff

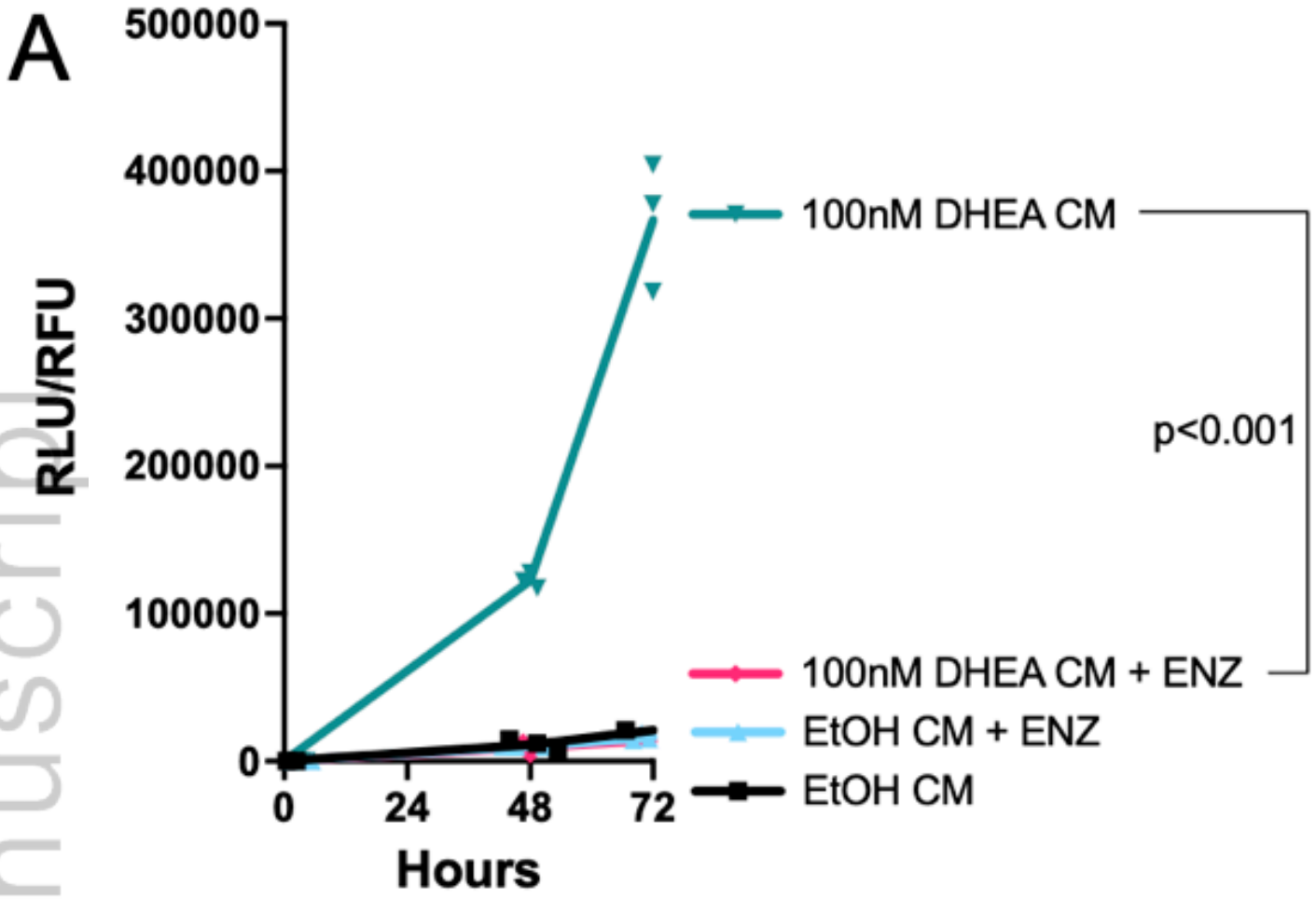


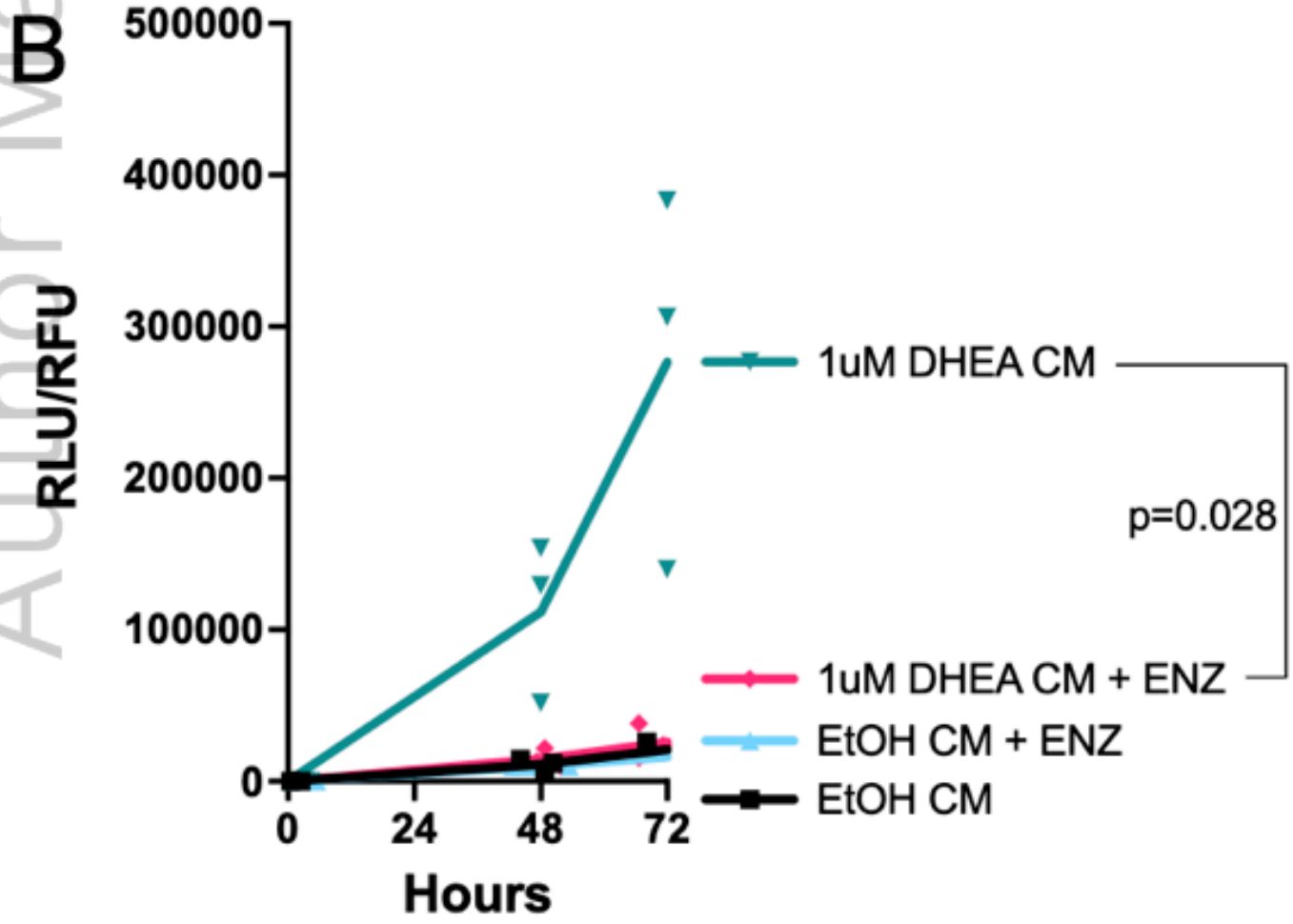


JBMR_4313_Figure 7.tiff

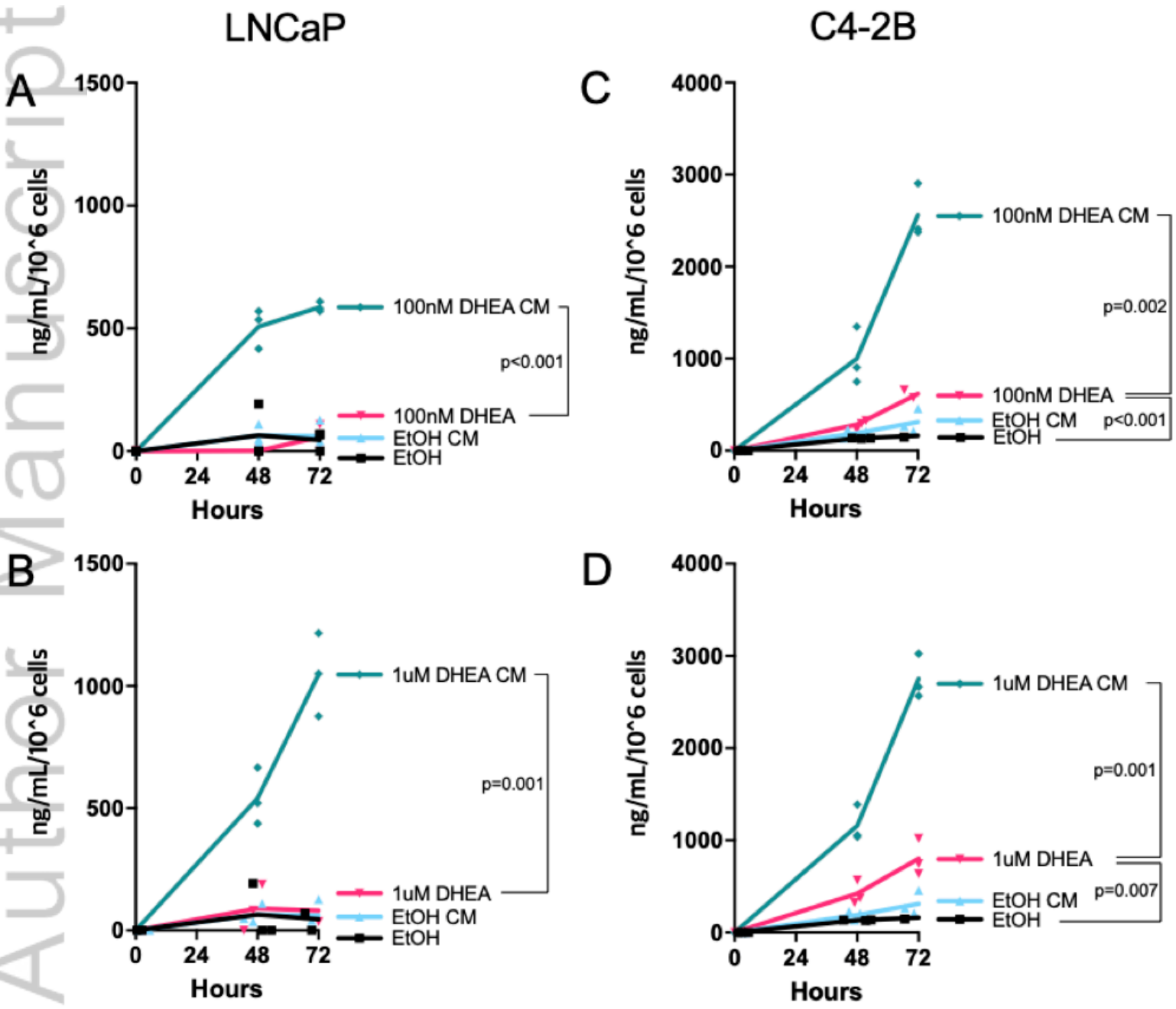


JBMR_4313_Figure 8.tiff

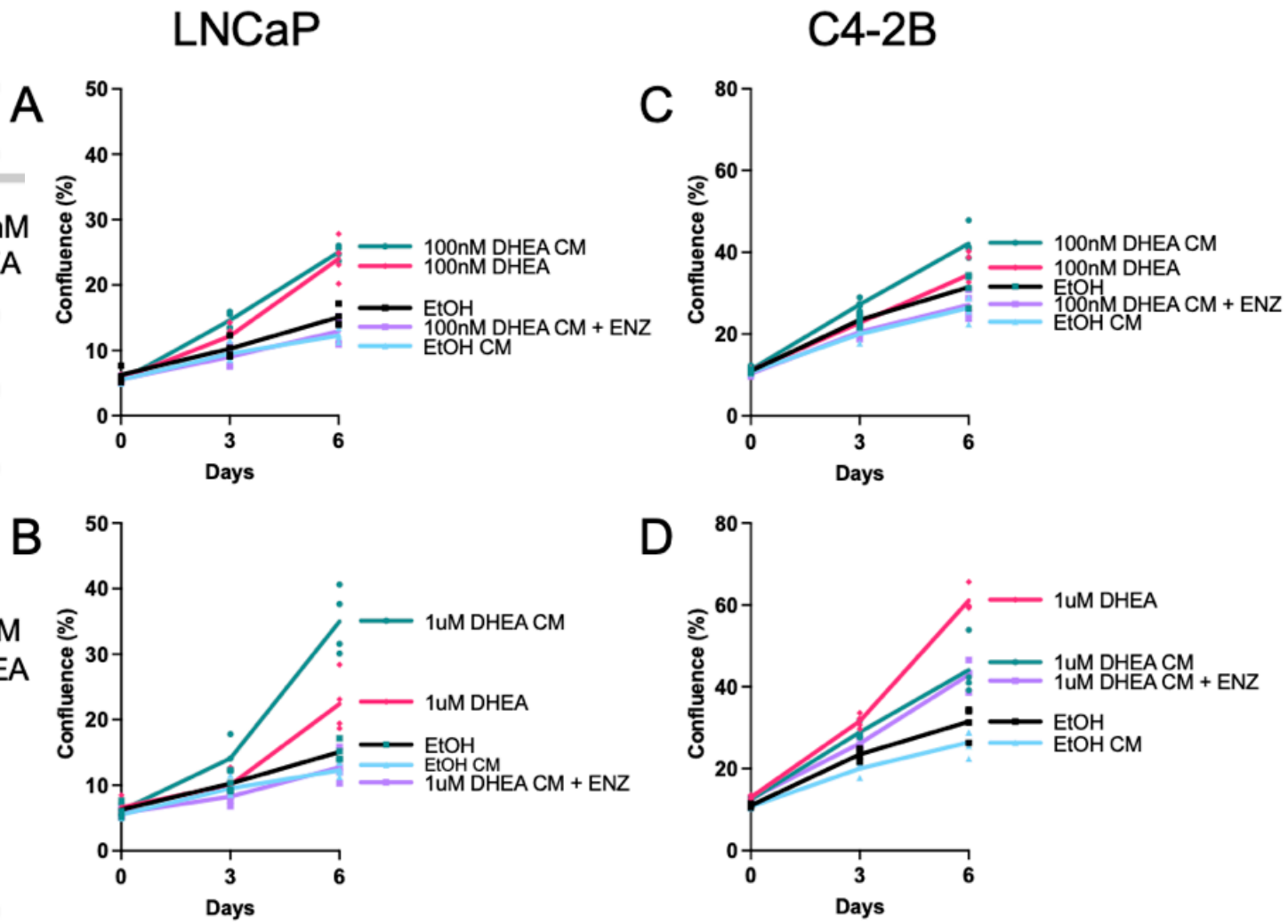


E

| Pairwise treatment comparisons vs. | | p value LNCaP | p value C4-2B |
|---|---|---|---|
| EtOH CM | 100 nM DHEA CM | **<0.001** | **0.001** |
| 100 nM DHEA CM | 100 nM DHEA CM + ENZ | **<0.001** | **0.001** |
| EtOH CM | 1 μM DHEA CM | **<0.001** | **0.002** |
| 1 μM DHEA CM | 1 μM DHEA CM + ENZ | **<0.001** | >0.1 |
| 100 nM DHEA CM | 1 μM DHEA CM | **0.034** | >0.1 |
| 100 nM DHEA | 100 nM DHEA CM | >0.1 | **0.040** |
| 1 μM DHEA | 1 μM DHEA CM | **0.020** | **0.007** |

JBMR_4313_Figure 9.tiff

A

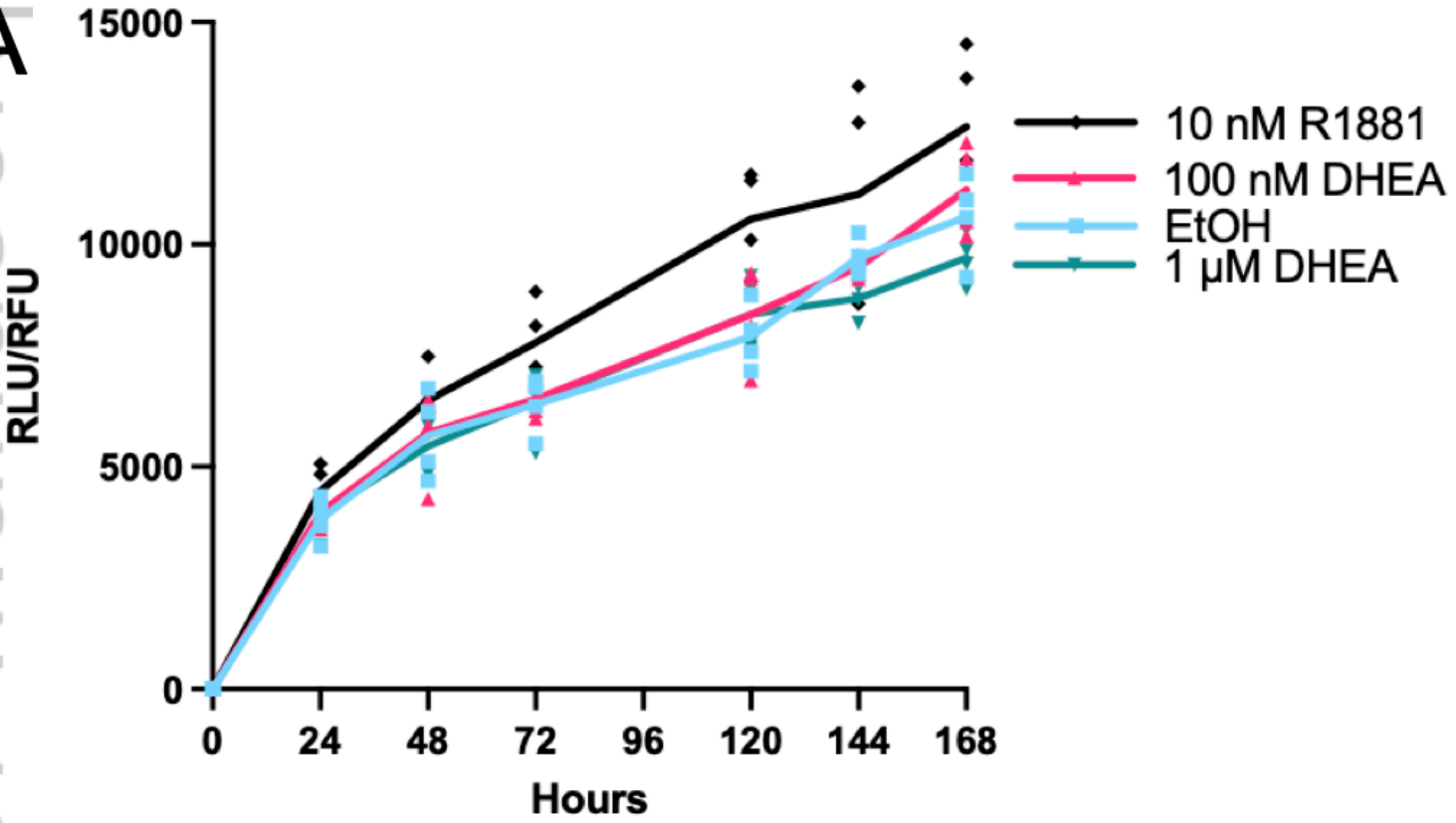


B

| Pairwise treatment comparisons | | p value |
|---|---|---|
| vs. | | |
| EtOH | 10 nM R1881 | **0.028** |
| EtOH | 100 nM DHEA | >0.1 |
| EtOH | 1 µM DHEA | >0.1 |

JBMR_4313_Figure 10.tiff